Laminar Flow in Microchannels With Noncircular Cross Section

Ali Tamayol
e-mail: ali_tamayol@sfu.ca

Majid Bahrami

Mechatronic Systems Engineering,
School of Engineering Science,
Simon Fraser University,
Surrey, BC, V3T0A3, Canada

Analytical solutions are presented for laminar fully developed flow in micro-/minichannels of hyperelliptical and regular polygonal cross sections in the form of compact relationships. The considered geometries cover a wide range of common simply connected shapes including circle, ellipse, rectangle, rectangle-with-round-corners, rhombus, star-shape, equilateral triangle, square, pentagon, and hexagon. A point matching technique is used to calculate closed form solutions for the velocity distributions in the above-mentioned channel cross sections. The developed relationships for the velocity distribution and pressure drop are successfully compared with existing analytical solutions and experimental data collected from various sources for a variety of geometries, including polygonal, rectangular, circular, elliptical, and rhombic cross sections. The present compact solutions provide a convenient and power tool for performing hydrodynamic analyses in a variety of fundamental and engineering applications such as in microfluidics, transport phenomena, and porous media. [DOI: 10.1115/1.4001973]

1 Introduction

The fast growth of microfluidic systems and their applications in microelectronic cooling [1], micro electro mechanical systems (MEMS) [2], fuel cell technology [3], microreactors [4], and medical and biomedical devices [5] has motivated many researchers to investigate microscale transport phenomena. Microchannels have specific characteristics such as high surface area per unit volume and high heat transfer coefficient [2]. Moreover, microchannels are essential components of many microfluidic devices and new compact thermal solutions [1]. In addition, porous materials can be modeled as networks of microscale conduits; thus, transport properties of porous structures are closely related to the geometry of the considered microchannels [6,7]. Recently, microchannels with different cross-sectional geometries were fabricated for both commercial and scientific purposes. Therefore, investigation of fluid flow in channels with different cross sections is important. Experimental studies conducted by Pfahler et al. [8,9], Harley et al. [10], Choi et al. [11], Stanley [12], and Gao et al. [13,14] confirmed that the continuum theory holds in micron size channels. Comprehensive reviews presented by Steinke and Kandlikar [15] and Papautsky et al. [16] have discussed this subject; thus, existing solutions for large scale ducts are also applicable to microchannels.

Several analytical solutions for flow in noncircular channels are available in literature. Dryden et al. [17] based on the analogy between fully developed velocity profile and stress function in elasticity reported velocity distribution in rectangular channels. Purday's model [18] presented a simple approximation for velocity distribution and Truskey et al. [19] employed separation of variable technique and developed exact velocity distribution in rectangular ducts. Solutions of flow in equilateral and isosceles triangular conduits are presented by Refs. [17,20], respectively. An isosceles trapezoid is an important shape since this cross section is formed as a result of etching process in silicon wafers [21]. Shah [22], employing a discrete least method, obtained solutions for fully developed flow in a variety of geometries including trapezoidal, triangular with and without round corners, and rhombic cross sections. Leveque solution for flow in an elliptical duct is reported by Richardson [23]. Cheng [24] employed nine point matching method to determine the velocity profile and Poiseuille number for m-sided regular polygonal ducts. Fully developed flow in ducts with several irregular cross sections are also solved, see, for example, Refs. [25–28]. The pertinent literature is reviewed critically by Shah and London [29]. The important point regarding the abovementioned solutions is that the forms of the final solutions are different from each other and is limited to the designated geometry.

The major drawback in using microsystems is their high pressure drop, resulted from their small cross-sectional length scale [30]. Bahrami et al. [31,32] developed a general model for predicting pressure drop in microchannels of arbitrary cross section. Using the analytical solution for elliptical duct and the concept of Saint-Venant principal in torsion, they showed that the Poiseuille number, f Re, where f is the Fanning friction factor and Re is the Reynolds number, is a function of the polar moment of inertia, area, and perimeter of the cross section of the channel. Their model showed good agreement with experimental and numerical data for a wide variety of cross sections such as rectangular, trapezoidal, triangular, circular, and moon shaped. However, they did not provide the velocity distribution in the considered microchannels.

An in-depth knowledge of velocity distribution plays a key role in determining other transport properties of microchannels such as heat and mass transfer coefficients. However, the authors were not able to find any general solutions for fully developed flow in ducts. As such, having a generalized solution for the velocity distribution in microchannels is a great value and can help to develop generalized models for prediction of heat and mass transfer rates in mini-/microchannels; this is the subject of the present work.

Regular polygon and hyperellipse are flexible geometries that can cover a wide range of simply connected shapes, such as square, triangle, hexagon, rectangle, ellipse, rhombus, and star shaped. Therefore, the solution of flow through polygonal and hyperelliptical channels will be valid for a wide range of common geometries, thus can be considered as a general solution.

In this study, an analytical solution is developed to predict the velocity distribution and the pressure drop of fully developed laminar flow in both hyperelliptical and polygonal mini-/microchannels. The proposed solution is validated through comparison with existing theoretical models and experimental data collected from different sources for a variety of geometries, including circular, rectangular, elliptical, triangular, and rhombic cross sections.

Contributed by the Fluids Engineering Division of ASME for publication in the JOURNAL OF FLUIDS ENGINEERING. Manuscript received November 18, 2009; final manuscript received June 1, 2010; published online: November 3, 2010. Assoc. Editor: Neelesh A. Patankar.

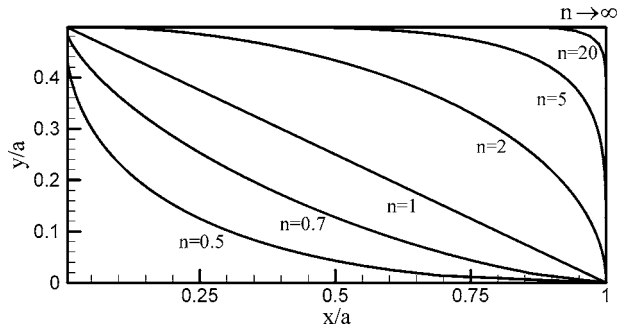

Fig. 1 Effect of *n* on the shape of the hyperellipse equation in the first quadrant, $\varepsilon=0.5$

2 Considered Geometries

2.1 Hyperellipse. In the first quadrant, a hyperellipse is described by

$$r_0 = \frac{a}{((\cos\theta)^n + (\sin\theta/\varepsilon)^n)^{1/n}}, \quad 0 < \varepsilon = \frac{b}{a} \leq 1 \tag{1}$$

where ε is the aspect ratio, and a and b are the major and minor axes of the cross section, respectively. As shown in Figs. 1 and 2, by varying parameter n, one can create several geometries. For $n<1$, the resulting geometry is a cross section with convex sides, i.e., star-shaped geometry. Equation (1) with $n=1$ results in a rhombus and when $n=2$ yields an ellipse; for $a=b$, the consequent geometry is a circle. For $n>2$, a rectangle with round corners is created and when $n\to\infty$ the resulting geometry becomes a rectangle; in the special case of $a=b$, it represents a square and for $a \ll b$ it yields parallel plates. Due to manufacturing processes, some of the flow passages have round corners. The hyperellipse geometry also covers these cross sections. The cross-sectional area of a hyperellipse can be calculated from [33]

$$A = 4a^2\varepsilon \frac{\sqrt{\pi}\Gamma\left(\frac{n+1}{n}\right)}{4^{1/n}\Gamma\left(\frac{n+2}{2n}\right)} \tag{2}$$

where $\Gamma(.)$ is the gamma function. The perimeter of the hyperellipse does not have a closed form solution and must be calculated from the following integral:

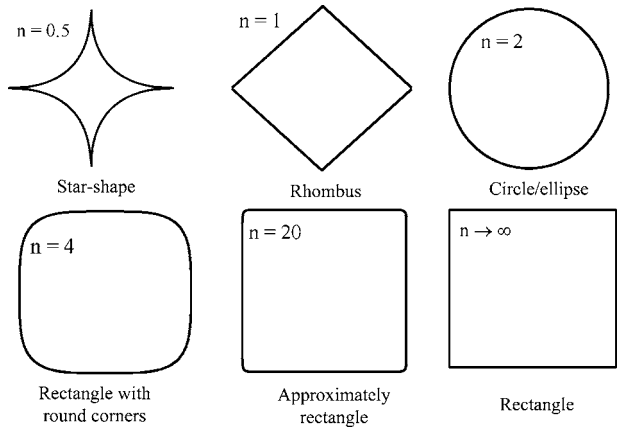

Fig. 2 Different geometries covered by hyperellipse geometry, $\varepsilon=1$

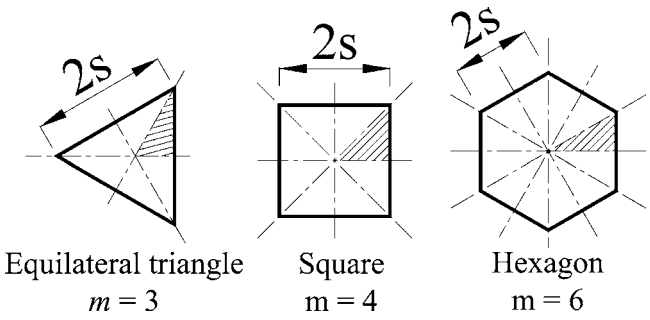

Fig. 3 Regular polygons with different number of sides, *m*

$$\Gamma_c = 4\int_0^{\pi/2} \sqrt{\left(\frac{dr_0}{d\theta}\right)^2 + r_0^2}\, d\theta \tag{3}$$

2.2 Regular polygon. As shown in Fig. 3, the m-sided regular polygon ducts covers a wide range of geometries. For $m=3$, the consequent geometry is an equilateral triangle; when $m=4$ and 6, the shapes become a square and a hexagon, respectively. A circle is a polygon with infinite number of sides, i.e., $m\to\infty$. The cross-sectional area of the polygonal channels is

$$A = \frac{ms^2}{\tan\frac{\pi}{m}} \tag{4}$$

and its perimeter is calculated as

$$\Gamma_c = 2ms \tag{5}$$

As shown in Fig. 3, all of the hatched regions surrounded by symmetry lines are triangles with different vertex angles.

3 Problem Formulation

Fully developed, laminar, constant properties, and incompressible flow in microchannels with constant hyperelliptical and polygonal cross sections is considered. The compressibility effects

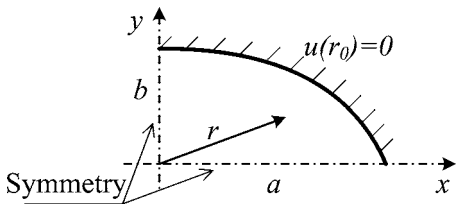

Fig. 4 Hyperelliptical cross-section and the boundary conditions

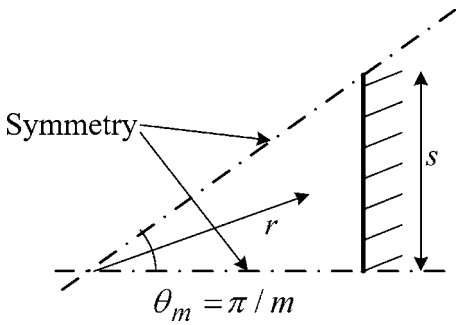

Fig. 5 Considered geometry for modeling regular polygonal cross section

Table 1 Coefficients for velocity distribution, Eq. (10) for hyperelliptical ducts

	$n=20$, rectangle						
	$\varepsilon=0.2$	$\varepsilon=0.25$	$\varepsilon=0.4$	$\varepsilon=0.5$	$\varepsilon=0.6$	$\varepsilon=0.8$	$\varepsilon=1$
A_1	0.020	0.031	0.077	0.114	0.153	0.229	0.295
C_1	0.250	0.248	0.225	0.195	0.158	0.076	0.000
C_2	−0.004	−0.010	−0.033	−0.045	−0.052	−0.053	−0.045
C_3	−0.002	−0.002	−0.012	−0.013	−0.010	−0.004	0.000
C_4	−0.007	−0.018	−0.010	−0.004	0.000	0.002	0.001
C_5	−0.006	0.001	0.004	0.003	0.001	0.000	0.000
	$n=4$, rectangle with round corners						
	$\varepsilon=0.2$	$\varepsilon=0.25$	$\varepsilon=0.4$	$\varepsilon=0.5$	$\varepsilon=0.6$	$\varepsilon=0.8$	$\varepsilon=1$
A_1	0.020	0.031	0.076	0.112	0.149	0.223	0.287
C_1	0.248	0.244	0.217	0.186	0.149	0.071	0.000
C_2	−0.016	−0.021	−0.037	−0.043	−0.045	−0.042	−0.035
C_3	0.013	0.009	0.003	0.001	0.001	0.000	0.000
C_4	−0.014	−0.012	−0.007	−0.005	−0.004	−0.002	−0.001
	$n=2$, ellipse						
	$\varepsilon=0.2$	$\varepsilon=0.25$	$\varepsilon=0.4$	$\varepsilon=0.5$	$\varepsilon=0.6$	$\varepsilon=0.8$	$\varepsilon=1$
A_1	0.019	0.029	0.069	0.100	0.132	0.195	0.250
C_1	0.231	0.221	0.181	0.150	0.118	0.055	0.000

$$A_1 = \frac{0.508\varepsilon^{1.99}}{1.302 + \varepsilon^{1.99}},\quad C_1 = 0.25 - A_1$$

	$n=1$, rhombus						
	$\varepsilon=0.2$	$\varepsilon=0.25$	$\varepsilon=0.4$	$\varepsilon=0.5$	$\varepsilon=0.6$	$\varepsilon=0.8$	$\varepsilon=1$
A_1	0.015	0.022	0.046	0.064	0.082	0.116	0.147
C_1	0.167	0.149	0.106	0.083	0.062	0.028	0.000
C_2	0.356	0.344	0.242	0.189	0.154	0.114	0.091
C_3	−1.130	−0.996	−0.453	−0.228	−0.110	−0.026	0.000
C_4	2.026	1.771	0.766	0.357	0.152	0.029	0.010
C_5	−1.792	−1.588	−0.728	−0.354	−0.155	−0.011	0.000
C_6	0.607	0.548	0.270	0.139	0.066	0.000	0.000
	$\varepsilon=1$, star-shape						
	$n=0.9$	$n=0.8$	$n=0.7$	$n=0.6$			
A_1	0.128	0.107	0.085	0.062			
C_1	0.000	0.000	0.000	0.000			
C_2	0.116	0.152	0.207	0.303			
C_3	0.000	0.000	0.000	0.000			
C_4	0.006	−0.008	−0.042	−0.176			
C_5	0.000	0.000	0.000	0.000			
C_6	0.000	0.000	0.000	0.061			

can be neglected for the Mach numbers lower than 0.3 [34]; thus, the present analysis is acceptable for all Newtonian liquids and gas flows with $Ma<0.3$. Using the abovementioned assumptions, the momentum equation reduces to Poisson's equation [34]:

$$\frac{dP}{dz} = \mu\left(\frac{\partial^2 u}{\partial r^2} + \frac{1}{r}\frac{\partial u}{\partial r} + \frac{1}{r^2}\frac{\partial^2 u}{\partial \theta^2}\right) \tag{6}$$

where μ is the fluid viscosity. Using the geometrical symmetry,

Table 2 Coefficients for velocity distribution, Eq. (13) for regular polygonal ducts

	$m=3$	$m=4$	$m=5$	$m=6$	$m=7$	$m=8$	$m=12$	$m\to\infty$
A_1	0.333	0.296	0.278	0.270	0.265	0.261	0.255	0.250
C_1	−0.083	−0.046	−0.03	−0.021	−0.015	−0.012	−0.006	0.000

$$u^* = \left[1 - \frac{\eta^2}{4A_1} + \sum_{i=1}^{\infty}\frac{C_i}{A_1}(\eta^{mi}\cos m\theta)\right],\quad A_1 = 0.247 + \frac{0.767}{m^2},\quad C_1 = \frac{1}{6.01 - 3.12m - 0.965m^2}$$

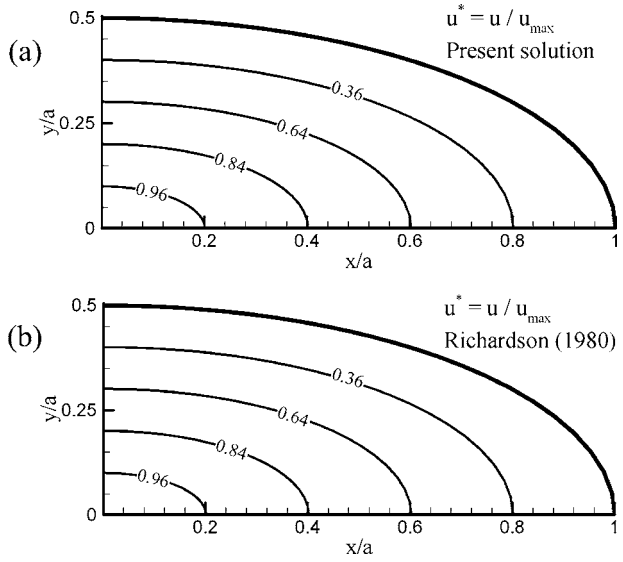

Fig. 6 Contours of constant velocity for elliptical channel with $\varepsilon=0.5$, (*a*) present model, Eq. (10); (*b*) model of Richardson et al. [23]

only a portion of the cross section is considered in the analysis, as shown in Figs. 4 and 5. Applicable boundary conditions for hyperelliptical channels are

$$\left.\frac{\partial u}{\partial \theta}\right|_{\theta=\pi/2} = 0, \qquad \left.\frac{\partial u}{\partial \theta}\right|_{\theta=0} = 0, \quad u(r_0) = 0 \tag{7}$$

The first two equations are obtained from the existing symmetry in the hyperellipse geometry. Moreover, the velocity should be bounded. The general solution of Poisson's equation, Eq. (6), in the cylindrical coordinate is [35]

$$u = A_0 + B \ln r - \frac{r^2}{4\mu}\left(\frac{dP}{dz}\right) + \sum_{k=1}^{\infty} (C_k r^k + D_k r^{-k})(E_k \cos k\theta + F_k \sin k\theta) \tag{8}$$

The unknown coefficients A_0, B, C_k, D_k, E_k, and F_k should be calculated by applying the boundary conditions, Eq. (7). At $r=0$, the velocity must have a finite value; thus, $B=D_k=0$. Since dP/dz remains constant for fully developed flows, Eq. (5) can be simplified as

$$u = \frac{1}{\mu}\left(\frac{dP}{dz}\right)\left[A_1 - \frac{r^2}{4} + \sum_{k=1}^{\infty} (r^k)(E_k \cos k\theta + F_k \sin k\theta)\right] \tag{9}$$

where A_1, E_k, and F_k are redefined. The symmetry conditions at $\theta=0$ and $\theta=\pi/2$ result in $F_k=0$ and $k=2,4,6,\ldots$, respectively. After nondimensionalizing, Eq. (9) reduces to

$$u^* = \left[1 - \frac{\zeta^2}{4A_1} + \sum_{i=1}^{\infty} \frac{C_i}{A_1}(\zeta^{2i} \cos 2i\theta)\right] \tag{10}$$

$$u^* = \frac{u}{U_{max}} = \frac{u}{\frac{1}{\mu}\left(-\frac{dP}{dz}\right)A_1 a^2}, \quad \zeta = \frac{r}{a}$$

The last boundary condition, i.e., the no-slip condition, $u^*(\eta_0)=0$, on the channel wall should be used to calculate the rest of unknown coefficients in Eq. (10). Substituting for η_0 from Eq. (1), one can write

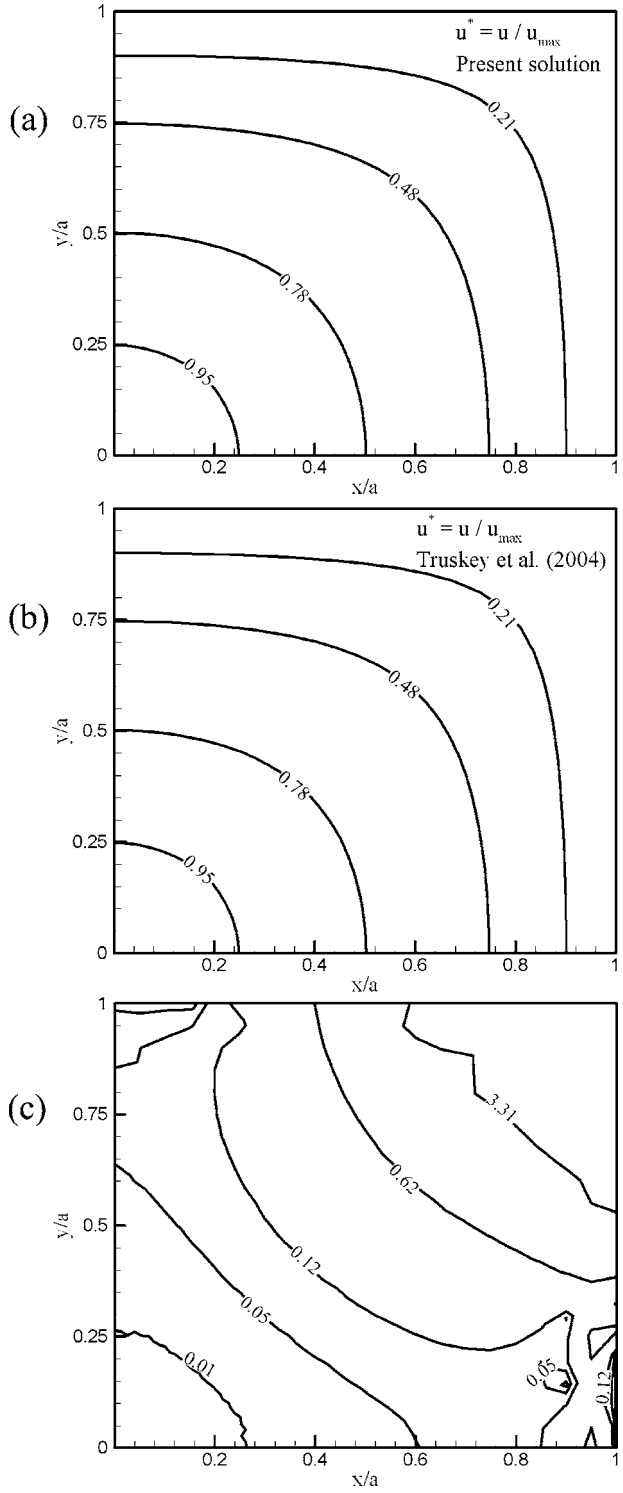

Fig. 7 Contours of constant velocity for squared channel, (*a*) present model, Eq. (10); (*b*) Truskey et al. [19]; (*c*) the relative percentage difference between the present model and the model of Truskey et al. [19]

$$A_1 - \frac{1}{4}\frac{1}{((\cos\theta)^n + (\sin\theta/\varepsilon)^n)^{2/n}} + \sum_{i=1}^{\infty} C_i\left(\frac{\cos 2i\theta}{((\cos\theta)^n + (\sin\theta/\varepsilon)^n)^{2i/n}}\right) = 0 \tag{11}$$

This equation is a function of θ. To evaluate the coefficients,

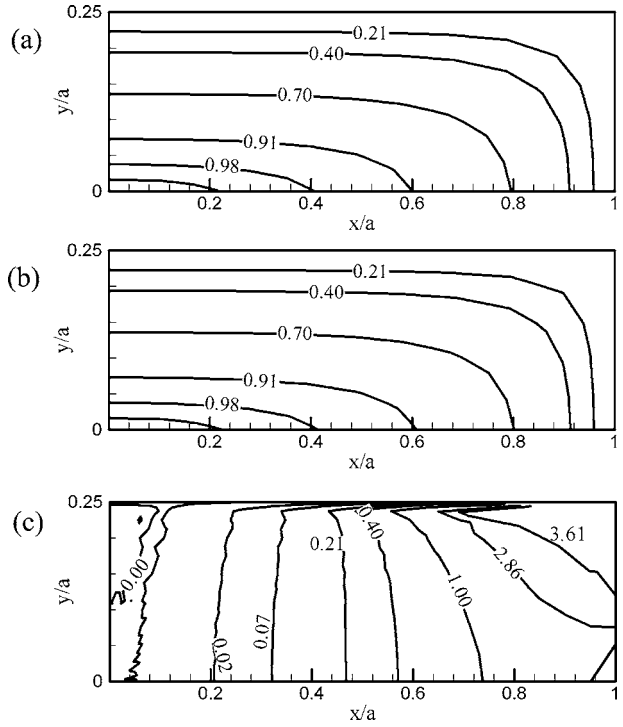

Fig. 8 Contours of constant velocity for rectangular channel with $\varepsilon=0.25$, (*a*) present model, Eq. (10); (*b*) Truskey et al. [19]; (*c*) the relative percentage difference between the present model and the model of Truskey et al. [19]

following Ref. [36], we truncate the series from the qth term and apply Eq. (11) over $q+1$ different θs and solve the resulting set of linear equations.

The same approach can be followed for polygonal ducts, shown in Fig. 5. The difference between the two geometries is the location of the symmetry lines. Applicable symmetry boundary conditions for polygonal cross section are

$$\left.\frac{\partial u}{\partial \theta}\right|_{\theta=\pi/m}=0, \qquad \left.\frac{\partial u}{\partial \theta}\right|_{\theta=0}=0 \tag{12}$$

where m is the number of sides. Using Eq. (12), the dimensionless velocity distribution becomes

$$u^*=\left[1-\frac{\eta^2}{4A_1}+\sum_{i=1}^{\infty}\frac{C_i}{A_1}(\eta^{mi}\cos m\theta)\right] \tag{13}$$

$$u^*=\frac{u}{U_{\max}}=\frac{u\left(\tan\frac{\pi}{m}\right)^2}{\frac{1}{\mu}\left(-\frac{dP}{dz}\right)A_1 s^2}, \qquad \eta=\frac{r\tan\frac{\pi}{m}}{s}$$

Applying no-slip boundary condition, the unknown coefficients in Eqs. (10) and (13) can be determined. The calculated coefficients for several hyperelliptical and polygonal ducts are listed in Tables 1 and 2, respectively.

A point matching technique [36] is used to apply the no-slip boundary condition to a finite number of points over the channel's wall in order to determine the coefficients in the velocity distribution, Eqs. (10) and (13). The series solution is then truncated to the same number of terms and the coefficients are reported in Tables 1 and 2. The number of terms in the recommended truncated solutions is determined such that a maximum relative difference of 5% with the full solution is achieved. It should be noted that the proposed velocity distributions are in the cylindrical coordinate, for cross sections that significantly deviate from the "elliptical shape," e.g., channels with sharp corners, more terms are included in the solution. The no-slip condition points are distributed over the entire channel's wall; however, more points are chosen near the corners to ensure a continuous no-slip condition.

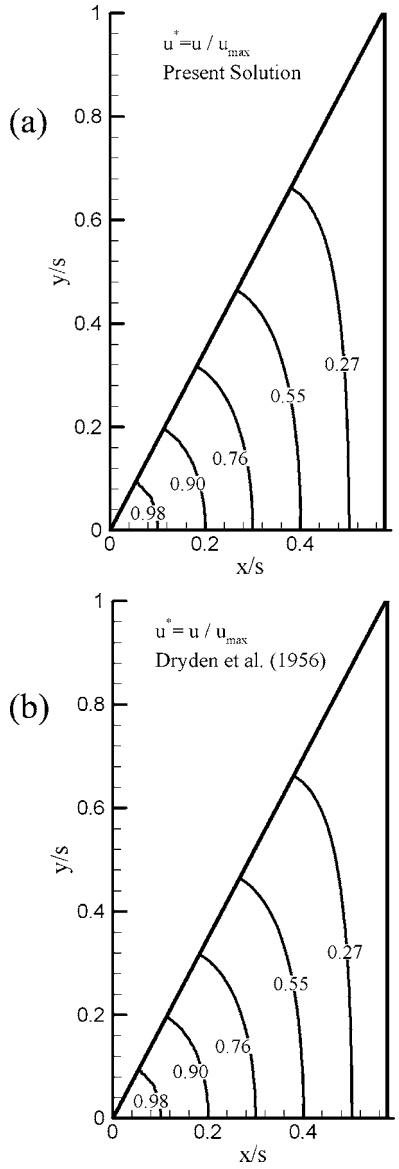

Fig. 9 Contours of constant velocity for a sector of triangular channel, (*a*) present model, Eq. (13); (*b*) the model of Dryden et al. [17]

To verify the present approach, in Figs. 6–8 the predicted nondimensional velocity distributions for elliptical and rectangular cross sections are compared with the analytical solutions of Richardson [23] and Truskey et al. [19], respectively. The hyperellipse equation, Eq. (1), for $n\to\infty$ yields a rectangle; however, $n=20$ is large enough to produce comparable results, see Fig. 1. Figures 6–8 show that the predicted contours of constant nondimensional velocities are in full agreement with the analytical results for both elliptical and rectangular cross sections. The solution for a polygonal duct with three sides, i.e., equilateral triangular, is successfully compared with the solution of Dryden et al. [17] in Fig. 9. The maximum velocities in the channel are also compared with the analytical results for the considered geometries in Table 3. Tabulated results justify the accuracy of the developed solution.

The solution for channels of star shaped and rectangular with round corners cross sections cannot be found elsewhere. The

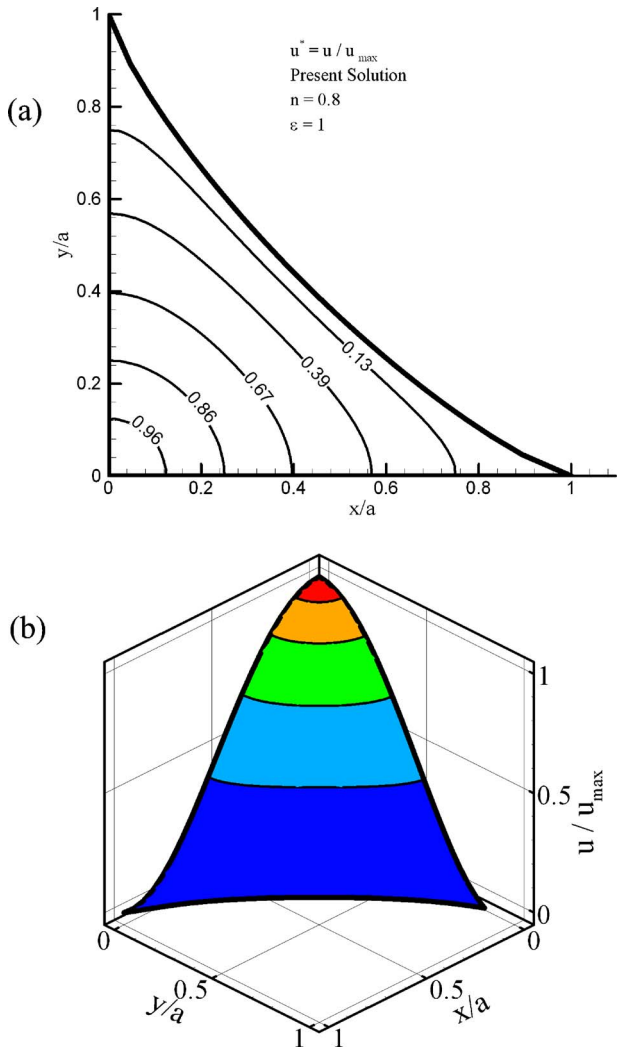

Fig. 10 Velocity contours and velocity distribution in a star-shaped channel with n=0.8 and ε=1, using Eq. (10)

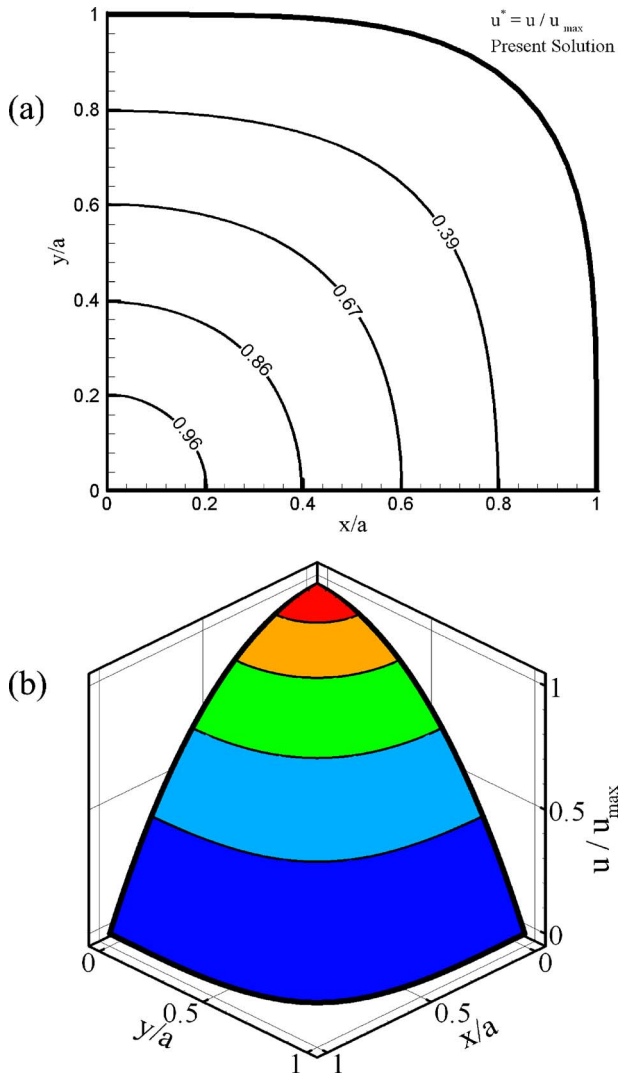

Fig. 11 Velocity contours and velocity distribution in a square with round corners duct, n=4, using Eq. (10)

former one has application in analyzing foams and packed beds, while the latter one is frequently formed during microfabrication process of rectangular microchannels. The velocity contours and distributions are plotted for ducts with star shaped and square with round corners cross sections in Fig. 10 and 11, respectively.

4 Pressure Drop and Poiseuille Number

Pressure drop is an important characteristic of any system that should be considered in the design procedure. Once the coefficients are known, one can integrate Eqs. (10) and (13) to find the pressure drop for a specific volumetric flow rate, Q, for hyperelliptical and polygonal ducts, respectively:

$$\left(-\frac{dP}{dz}\right)_{\text{hyperellipse}} = \frac{\mu Q}{a^2}\left\{\int\int\left[A_1 - \frac{\zeta^2}{4} + \sum_{i=1}^{\infty} C_i(\zeta^{2i}\cos 2i\theta)\right]dA\right\}^{-1} \tag{14}$$

Table 3 Comparison between the calculated maximum velocities in elliptical and rectangular channels with other analytical solutions

	Elliptical cross-section [23]	n=2 (present solution)	Rectangular cross-section [19]	n=20 (present solution)
ε=1	0.2500	0.2500	0.2947	0.2946
ε=0.5	0.1000	0.1000	0.1139	0.1138
ε=0.33	0.0500	0.0500	0.0545	0.0545
ε=0.25	0.0294	0.0294	0.0311	0.0311
ε=0.2	0.0192	0.0192	0.0200	0.0200

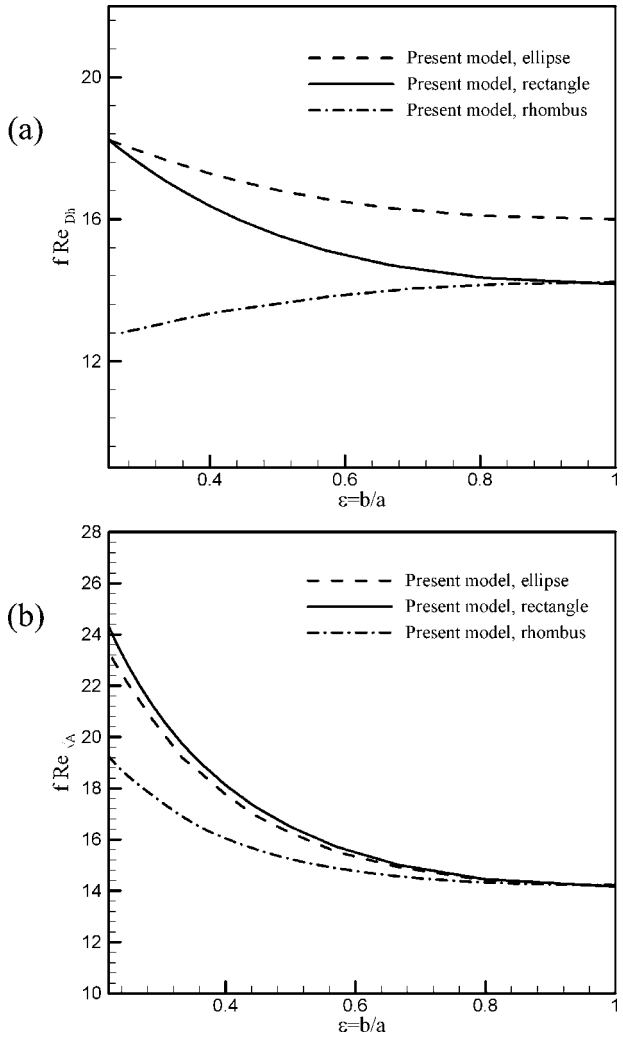

Fig. 12 *f* Re for different geometries using (a) hydraulic diameter and (b) square root of cross-sectional area as characteristic length scales

$$\left(-\frac{dP}{dz}\right)_{\text{polygon}} = \frac{\mu Q\left(\tan\frac{\pi}{m}\right)^2}{s^2}\left\{\int\int\left[A_1 - \frac{\eta^2}{4} + \sum_{i=1}^{\infty} C_i(\eta^{mi}\cos mi\theta)\right]dA\right\}^{-1} \quad (15)$$

It can be seen that the pressure drop is a function of the volumetric flow rate and dimensions of the cross section. Poiseuille number, f Re, is the common dimensionless number used for analyzing pressure drop in channels. The value of f Re depends on the characteristic length scale used for defining the Reynolds number. It should be noted that selection of the characteristic length does not affect the calculated pressure drop. However, a more appropriate length scale leads to more consistent results, especially when various cross sections are considered. A circular duct is fully described with its diameter; thus the obvious length scale is the diameter (or radius). For noncircular cross sections, the selection is not as clear; many textbooks and researchers have conventionally chosen the hydraulic diameter [34]. Figures 12(*a*) and 12(*b*) show the comparison of the analytical solutions of f Re, for elliptical, rectangular, and rhombus cross sections based on the hydraulic diameter and the square root of area, respectively. It can be observed that using the square root of area as the characteristic length leads to similar trends in analytical solutions of f Re for the considered geometries. The values of $f\,\mathrm{Re}_{\sqrt{A}}$ can be determined from the following equation:

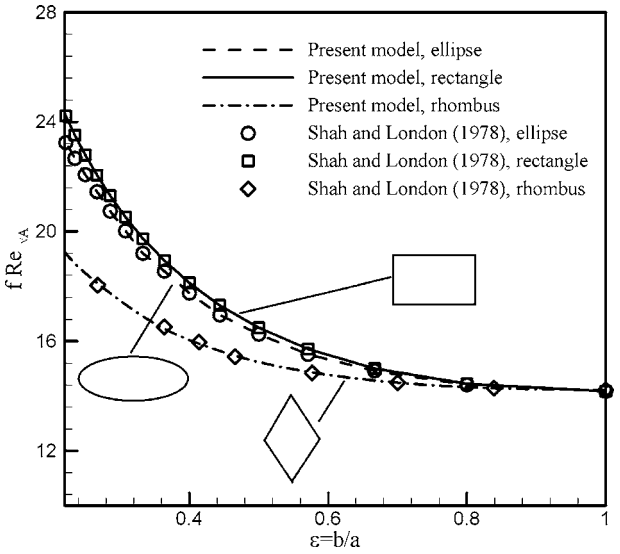

Fig. 13 Values of *f* $\mathrm{Re}_{\sqrt{A}}$ obtained from present model, Eq. (16), and existing correlations [29] for different values of *n*, hyperelliptical ducts

$$f\,\mathrm{Re}_{\sqrt{A}} = \frac{2A^{5/2}}{\mu Q\Gamma_c}\left(-\frac{dP}{dz}\right) \quad (16)$$

where Γ_c is the cross-section perimeter and dp/dz is calculated from Eqs. (14) and (15). Values of $f\,\mathrm{Re}_{\sqrt{A}}$ obtained from the present model and the correlations proposed by Shah and London [29] are plotted in Fig. 13 versus the cross-sectional aspect ratio for rectangular, elliptical, and rhombic ducts. The results have an excellent agreement. The rectangular microchannels have the highest $f\,\mathrm{Re}_{\sqrt{A}}$ in comparison to other considered geometries with the same cross-sectional area. In addition, it can be seen that the Poiseuille number has a reverse relationship with aspect ratio.

In Fig. 14, $f\,\mathrm{Re}_{\sqrt{A}}$ values for polygonal channels calculated using the present solution are compared with the results of Shah

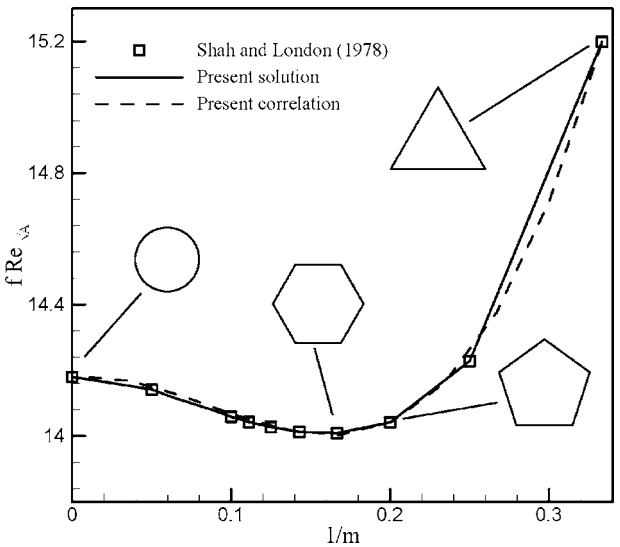

Fig. 14 Values of *f* $\mathrm{Re}_{\sqrt{A}}$ obtained from present model, Eq. (17), and tabulated values reported by [29] for different values of *m*, regular polygonal ducts

Table 4 $f\ \mathrm{Re}_{\sqrt{A}}$ **for elliptical ducts obtained from different models**

ε	$f\ \mathrm{Re}_{\sqrt{A}}$ [23]	$f\ \mathrm{Re}_{\sqrt{A}}$ (present solution)	$f\ \mathrm{Re}_{\sqrt{A}}$ [31]
1	14.18	14.18	14.18
0.5	16.26	16.26	16.26
0.33	19.20	19.20	19.20
0.25	22.07	22.07	22.07
0.2	24.65	24.65	24.65

and London [29] and the results are in complete agreement. More importantly, the minimum value of $f\ \mathrm{Re}_{\sqrt{A}}$ occurs for $m=6$; this means that hexagonal ducts have the minimum pressure drop in comparison with other polygonal shapes. It can be seen that the $f\ \mathrm{Re}_{\sqrt{A}}$ for regular polygonal channels can be calculated with less than 1% inaccuracy using the following equation:

$$f\ \mathrm{Re}_{\sqrt{A}} = 14.18 + 0.5m^{-1} - 26.4m^{-2} + 102.18m^{-3} \qquad (17)$$

To determine the Poiseuille number, $f\ \mathrm{Re}$, Bahrami et al. [30,31] started from the analytical solution of elliptical channel. They also selected $\sqrt{A}$ as the length scale in their study. The final result was presented in an easy-to-use form, as a function of cross-sectional area and polar moment of inertia. In Table 4 the nondimensional values of the pressure drop for elliptical ducts are compared with the analytical model of Richardson [23] and the model of Bahrami et al. [31]. All solutions capture the same results for elliptical channels. The values of the pressure drop obtained from the present solution for rectangular cross section and the approximate model of Bahrami et al. [31] are listed in Table 5. It can be seen that the difference between the proposed model and the model of Bahrami et al. [31] is less than 8%. Therefore, the model of Bahrami et al. [31] is an accurate alternative approach for prediction of approximate values of pressure drop.

4.1 Comparison With Experimental Data. Several researchers have reported experimental data for pressure drop in rectangular microchannels. Stanly [12] studied flow of water, nitrogen, and helium in arrays of rectangular microchannels. The channels were fabricated by machining aluminum substrates and then covering them with glass plates. Papautsky et al. [37] fabricated arrays of pipettes with width varying from 150 μm to 600 μm. Their data for low aspect ratios consistently were 20% larger than theoretical values. Therefore, only their results for aspect ratios larger than 0.05 are included here.

Liu and Garimella [38] carried out experiments and measured the friction factor in rectangular microchannels. They did not observe any scale-related phenomena in their experiments and concluded that the conventional theory can be used to predict the flow behavior in microchannels in the range of dimensions considered.

Wu and Cheng [39] conducted experiments and measured the friction factor of laminar flow of de-ionized water in smooth silicon microchannels of trapezoidal, rectangular, and triangular cross sections.

Jung and Kwak [40] experimentally measured fluid flow and heat transfer in rectangular silicon microchannels with different aspect ratios. But, they only reported the friction factor for two geometries, $\varepsilon=0.5$ and 1.

Table 5 $f\ \mathrm{Re}_{\sqrt{A}}$ **for rectangular ducts obtained from different models**

ε	$f\ \mathrm{Re}_{\sqrt{A}}$ (present solution)	$f\ \mathrm{Re}_{\sqrt{A}}$ [31]
1	14.17	13.16
0.5	16.50	15.51
0.33	19.74	18.99
0.25	22.79	22.37
0.2	25.60	25.50

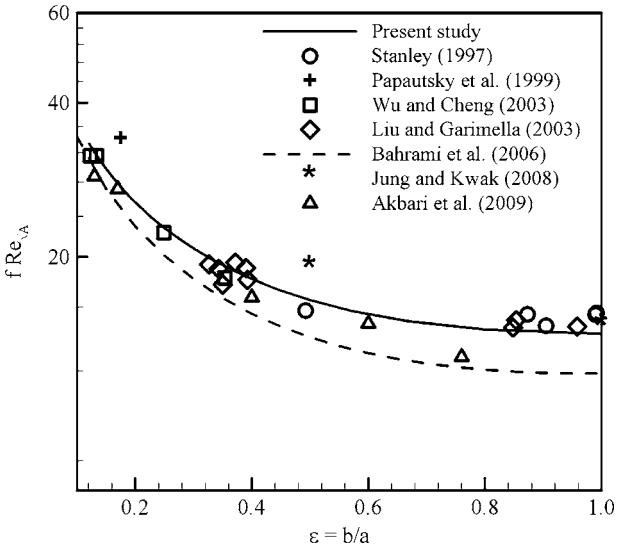

Fig. 15 Comparison of the $f\ \mathrm{Re}_{\sqrt{A}}$ **values for rectangular channels predicted using Eq. (16) with experimental data collected from various sources**

Recently, Akbari et al. [41] performed experiments to measure pressure drop in rectangular microchannels, fabricated in polydimethylsiloxane (PDMS). The fabricated channels were cut in different locations to make sure that they have a rectangular cross section. They tested several samples with a wide range of cross-sectional aspect ratios.

In Fig. 15, the values of Poiseuille number are plotted against experimental data collected from the above-mentioned sources. It can be seen that the present solution captures the trends of experimental data of liquid flow in rectangular ducts fabricated using different materials over a wide range of aspect ratios. Moreover, it can be seen that the model of Bahrami et al. [31] provides good approximations for Poiseuille number.

5 Conclusions

Analytical solutions were proposed for the laminar, fully developed flow through hyperelliptical and polygonal mini-/microchannels. The present method enables one to predict velocity distribution and pressure drop for several common fabricated geometries for industrial applications including circular, elliptical, rectangular, rhombus, triangular, and hexagonal ducts. The approach was based on using general solution Poisson's equation in the form of trigonometric series expansion. Therefore, the required coefficients were reported for a wide range of geometries. Using the developed solution for velocity distribution, pressure drops and Poiseuille numbers were determined for a variety of cross sections. The predicted values were verified through comparison with analytical solutions for elliptical, circular, rectangular, rhombic, and polygonal ducts. Predicted results were also successfully compared with experimental data collected by others for rectangular channels.

Acknowledgment

The authors gratefully acknowledge the financial support of the Natural Sciences and Engineering Research Council of Canada (NSERC).

Nomenclature

a = hyperellipse major axis, m
A = cross-sectional area, m^2
b = hyperellipse minor axis, m

D_h = hydraulic diameter, $4A/\Gamma_c$, m
f = Fanning friction factor
f Re = Poiseuille number
I_p = Polar moment of inertia about the centroid, m^4
m = number of sides in regular polygonal ducts
n = exponent in hyperellipse formula
P = pressure, N/m^2
Q = volumetric flow rate, m^3/s
Re = Reynolds number
s = half the length of the sides in polygonal ducts, m
u = axial velocity, m/s
u^* = nondimensional velocity, Eq. (7)

Greek symbols

$\Gamma(.)$ = gamma function
Γ_c = perimeter, m
ε = cross-sectional aspect ratio, $\varepsilon=b/a$
η = nondimensional coordinate, $\eta=r(\tan \pi/m)/s$
μ = viscosity, N s/m^2
θ = coordinate system
θ_m = half of the vertex angle in polygon with m sides
ζ = nondimensional coordinate, $\zeta=r/a$

Subscript

$\sqrt{A}$ = Square root of cross-sectional area, m

References

[1] Tuckerman, D. B., and Pease, R. F., 1981, "High-Performance Heat Sinking for VLSI," IEEE Electron Device Lett., **2**, pp. 126–129.
[2] Ho, C. M., and Tai, Y. C., 1998, "Micro-Electro-Mechanical-Systems (MEMS) and Fluid Flows," Annu. Rev. Fluid Mech., **30**, pp. 579–612.
[3] Cha, S. W., O'Hayre, R., and Prinz, F. B., 2004, "The Influence of Size Scale on the Performance of Fuel Cells," Solid State Ionics, **175**, pp. 789–795.
[4] Günther, A. l., Khan, S. A., Thalmann, M., Trachsel, F., and Jensen, K. F., 2004, "Transport and Reaction in Microscale Segmented Gas-Liquid Flow," Lab Chip, **4**, pp. 278–286.
[5] Effenhauser, C., Manz, A., and Widmor, M., 1993, "Glass Chips for High-Speed Capillary Electrophoresis Separation With Submicrometer Plate Heights," Anal. Chem., **65**, pp. 2637–2642.
[6] Kaviany, M., 1992, *Principles of Heat Transfer in Porous Media*, Springer-Verlag, New York.
[7] Tamayol, A., and Bahrami, M., 2009, "Analytical Determination of Viscous Permeability of Fibrous Porous Media," Int. J. Heat Mass Transfer, **52**, pp. 2407–2414.
[8] Pfahler, J., Harley, J., Bau, H., and Zemel, J. N., 1990, "Liquid Transport in Micron and Submicron Channels," Sens. Actuators, A, **A21–A23**, pp. 431–437.
[9] Pfahler, J., Harley, J., Bau, H., and Zemel, J. N., 1991, "Gas and Liquid Transport in Small Channels," Micromechanical Sensors, Actuators, and Systems, DSC Vol. 19, ASME, New York, pp. 49–58.
[10] Harley, J. C., Huang, Y., Bau, H., and Zemel, J. N., 1995, "Gas Flow in Microchannels," J. Fluid Mech., **284**, pp. 257–74.
[11] Choi, S. B., Barron, R. F., and Warrington, R. O., 1991, "Fluid Flow and Heat Transfer in Microtubes," ASME Micromechanical Sensors, Actuators, and Systems, DSC Vol. 32, pp. 123–134.
[12] Stanley, R. S., 1997, "Two-Phase Flow in Microchannels," Ph.D. thesis, Louisiana Tech University, Ruston, LA.
[13] Gao, P., Person, S. L., and Marinet, M. F., 2002, "Scale Effects on Hydrodynamics and Heat Transfer in Two-Dimensional Mini and Microchannels," Int. J. Therm. Sci., **41**, pp. 1017–1027.
[14] Cao, B., Chen, G. W., and Yuan, Q., 2005, "Fully Developed Laminar Flow and Heat Transfer in Smooth Trapezoidal Microchannel," Int. Commun. Heat Mass Transfer, **32**, pp. 1211–1220.
[15] Steinke, M. E., and Kandlikar, S. G., 2006, "Single-Phase Liquid Friction Factors in Microchannels," Int. J. Therm. Sci., **45**, pp. 1073–1083.
[16] Papautsky, I., Ameel, T., and Frazier, A. B., 2001 "A Review of Laminar Single Phase Flow in Microchannels," ASME International Mechanical Engineering Conference and Exposition, New York, Nov. 21–26.
[17] Dryden, H. L., Murnaghan, F. D., and Bateman, H., 1932, "*Hydrodynamics*," Dover, New York, pp. 197–201.
[18] Purday, H. F. P., 1949, *An Introduction to the Mechanics of Viscous Flow; Film Lubrication, the Flow of Heat by Conduction and Heat Transfer by Convection*, Dover, New York.
[19] Truskey, G. A., Yuan, F., and Katz, D. E., 2004, *Transport Phenomena in Biological Systems*, Pearson Prentice-Hall, Englewood Cliffs, NJ.
[20] Sparrow, E. M., 1962, "Laminar Flow in Isosceles Triangular Ducts," AIChE J., **8**, pp. 599–604.
[21] Sadasivam, R., Manglik, R. M., and Jog, M. A., 1999, "Fully-Developed Forced Convection Through Trapezoidal and Hexagonal Ducts," Int. J. Heat Mass Transfer, **42**, pp. 4321–4331.
[22] Shah, R. K., 1975, "Laminar Flow Friction and Forced Convection in Duct of Arbitrary Geometry," Int. J. Heat Mass Transfer, **18**, pp. 849–862.
[23] Richardson, S. M., 1980, "Leveque Solution for Flow in an Elliptical Duct," Lett. Heat Mass Transfer, **7**, pp. 353–362.
[24] Cheng, K. C., 1966, "Laminar Forced Convection in Regular Polygon Ducts With Uniform Peripheral Heat Flux," Proceedings of the Third International Heat Transfer Conference, New York, pp. 64–76.
[25] Ding, J., and Manglik, R. M., 1996, "Analytical Solutions for Laminar Fully-Developed Flows in Double-Sine Shaped Ducts," Heat Mass Transfer, **31**, pp. 269–277.
[26] Lee, Y.-M., and Chang, L. P., 2002, "Heat Transfer Coefficients of Laminar Flow in a Rhombic Duct With Constant Wall Temperature," Numer. Heat Transfer, **42**, pp. 285–296.
[27] Manglik, R. M., and Bergles, A. E., 1994, "Fully Developed Laminar Heat Transfer in Circular-Segment Ducts With Uniform Wall Temperature," Numer. Heat Transfer, **26**, pp. 499–519.
[28] Richardson, D. H., Sekulic, D. P., and Campo, A., 2000, "Low Reynolds Number Flow Inside Microchannels With Irregular Cross-Sections," Heat Mass Transfer, **36**, pp. 187–193.
[29] Shah, R. K., and London, A. L., 1978, *Laminar Flow Forced Convection in Ducts*, Academic, New York.
[30] Bahrami, M., Tamayol, A., and Taheri, P., 2009, "Slip-Flow Pressure Drop in Microchannels of General Cross-Section," ASME J. Fluids Eng., **131**, pp. 1036–1044.
[31] Bahrami, M., Yovanovich, M. M., and Culham, J. R., 2006, "Pressure Drop of Laminar, Fully Developed Flow in Microchannels of Arbitrary Cross-Section," ASME J. Fluids Eng., **128**, pp. 1036–1044.
[32] Bahrami, M., Yovanovich, M. M., and Culham, J. R., 2007, "A Novel Solution for Pressure Drop in Singly Connected Microchannels of Arbitrary Cross-Section," Int. J. Heat Mass Transfer, **50**, pp. 2492–2502.
[33] Yovanovich, M. M., Burde, S. S., and Thompson, J. C., 1976, "Thermal Constriction Resistance of Arbitrary Planar Contacts With Constant Flux," AIAA 11th Thermophysics Conference, San Diego, CA.
[34] White, F. M., 1984, *Viscous Fluid Flow*, McGraw-Hill, New York.
[35] Farlow, S. J., 1993, *Partial Differential Equations for Scientists and Engineers*, Dover, New York.
[36] Sparrow, E. M., and Loeffler, A. L., 1959, "Longitudinal Laminar Flow Between Cylinders Arranged in Regular Array," AIChE J., **5**, pp. 325–330.
[37] Papautsky, I., Gale, B. K., Mohanty, S., Ameelc, T. A., and Frazier, A. B., 1999, "Effects of Rectangular Microchannel Aspect Ratio on Laminar Friction Constant," SPIE Conference on Microfluidic Devices and Systems II, Santa Clara, CA.
[38] Liu, D., and Garimella, S., 2004, "Investigation of Liquid Flow in Microchannels," J. Thermophys. Heat Transfer, **18**, pp. 65–72.
[39] Wu, H. Y., and Cheng, P., 2003, "Friction Factors in Smooth Trapezoidal Silicon Microchannels With Different Aspect Ratios," Int. J. Heat Mass Transfer, **46**, pp. 2519–2525.
[40] Jung, J. Y., and Kwak, H. Y., 2008, "Fluid Flow and Heat Transfer in Microchannels With Rectangular Cross-Section," Heat Mass Transfer, **44**, pp. 1041–1049.
[41] Akbari, M., Bahrami, M., and Sinton, D., 2009, "Flow in Rectangular Microchannels: An Experimental Investigation," ASME J. Fluids Eng., **131**, p. 041202.